

α - α double folding cluster potential description of the $^{12}\text{C} + ^{24}\text{Mg}$ system

M. Karakoc and I. Boztosun

Department of Physics, Erciyes University, Kayseri, Turkey

(Received 28 September 2005; revised manuscript received 23 January 2006; published 5 April 2006)

We present a simultaneous analysis of the elastic scattering and fusion cross-section data of the $^{12}\text{C} + ^{24}\text{Mg}$ system around the Coulomb barrier and over energies by using the microscopic α - α double folding cluster potential within the framework of the optical model and the coupled-channels formalism. The α - α double folding cluster potential is obtained by using the α -cluster distribution densities of the nuclei in the usual double folding procedure. The microscopic potential results are compared with the findings of the phenomenological deep and shallow potentials. It is subsequently shown that only phenomenological deep, real, microscopic nucleon-nucleon and α - α double folding cluster potentials provide a consistent description of the angular distributions and fusion cross-section data simultaneously. The effect of the inclusion of the excited states of the target nucleus ^{24}Mg on the fusion cross-section predictions is also determined by the coupled-channels calculations, which are shown to improve the agreement.

DOI: [10.1103/PhysRevC.73.047601](https://doi.org/10.1103/PhysRevC.73.047601)

PACS number(s): 24.10.Ht, 21.60.Gx, 24.50.+g, 25.70.Jj

Determining the shape of the nuclear potential between two colliding pairs is a long-standing problem. Theoretical investigations of the precisely measured experimental data at high energies well over the Coulomb barrier for systems like $^{12}\text{C} + ^{12}\text{C}$ and $^{16}\text{O} + ^{16}\text{O}$ have led to the determination of the gross features of the local optical potentials. Subsequently, ambiguities have been clarified in many cases regarding the depths of the real parts of the nuclear potentials [1]. However, it is not yet possible to claim the same conclusive arguments for the shape of the nuclear potential for the reactions around the Coulomb barrier. The theoretical analysis suffers from a number of serious drawbacks such as the failure to determine the shape of the interaction potential, the reproduction of the oscillatory structure, and the out-of-phase problem between theoretical predictions and experimental data.

In this context, the $^{12}\text{C} + ^{24}\text{Mg}$ reaction [2–6] has been extensively investigated both experimentally and theoretically. The conventional optical model analysis conducted so far fails to explain all or some of the experimental data by using shallow or deep optical potentials [2–4]. Moreover, there has been no detailed microscopic study using folding models that attempts to explain the individual angular distributions and fusion cross-sections data simultaneously. Therefore, we aim to analyze the $^{12}\text{C} + ^{24}\text{Mg}$ system for energies from 16.0 to 24.0 MeV by using the α - α microscopic double folding cluster (DFC) potential. Our results are shown in comparison with the nucleon-nucleon double folding (NN-DF) potential and phenomenological shallow (WS_S) and deep (WS_D) real potentials.

In this Brief Report, we first introduce the potentials used in the optical model and coupled-channels (CC) formalism. Then the optical and CC results are shown and conclusions are drawn.

To make a comparative study of this reaction, we have used four different potentials for the real part of the optical model potential: Two are microscopic, which are calculated from microscopic NN-DF and α - α DFC potentials, and the other two are phenomenological deep and shallow potentials. We provide

the details of the α - α DFC potential and leave the NN-DF and phenomenological potentials to references provided in Refs. [2,7,8].

The projectile and target nuclei that we study in this Brief Report consist of an integer multiple of the number of α particles. It has been known that $4n$ -type nuclei have an α -cluster structure [9,10]. Therefore, it will be very interesting to obtain the interaction potential by considering the α -particle structure of these nuclei. For this purpose, the α - α DFC potential is constructed in a similar way to the ordinary DF one: We fold an α - α effective interaction with α -clusters distribution densities and formulate the nucleus-nucleus DFC optical model potential [11] as

$$V_{\text{DFC}}(r) = \iint \rho_{cP}(r_1)\rho_{cT}(r_2)v_{\alpha\alpha}(|\vec{r} + \vec{r}_2 - \vec{r}_1|)d^3r_1d^3r_2, \quad (1)$$

where ρ_{cP} and ρ_{cT} are the α -cluster distributions for projectile and target nuclei, respectively, and $v_{\alpha\alpha}$ is the effective α - α interaction.

The matter distribution of a nucleus is known and can be obtained from

$$\rho_M(r) = \rho_{0M}(1 + wr^2)\exp(-\beta r^2). \quad (2)$$

This is a modified form of the Gaussian shape for $\rho_M(r)$, the projectile and target densities. The matter density of an α nucleus can also be obtained from

$$\rho_\alpha(r) = \rho_{0\alpha}\exp(-\beta r^2). \quad (3)$$

The parameters for $\rho_{0\alpha}$, ρ_{0M} , w , and β used in Eqs. (2) and (3) are given in Table I.

If $\rho_c(r')$ is the α -cluster distributions function inside the nucleus, then we can relate the nuclear matter density distribution functions of the nucleus, $\rho_M(r)$, to that of the α -particle nucleus, $\rho_\alpha(r)$, as

$$\rho_M(r) = \int \rho_c(r')\rho_\alpha(|\vec{r} - \vec{r}'|)d^3r'. \quad (4)$$

Since the densities of the nucleus and the α particle can be calculated from Eqs. (2) and (3), by using Fourier transform

TABLE I. The parameters of nuclear matter densities of ^{12}C and ^4He [12]. The parameter of ^{24}Mg nuclear matter density is obtained from RIPL-2 [13].

Nuclei	ρ_0 (fm^{-3})	w (fm^{-2})	β (fm^{-2})	$\langle r^2 \rangle^{1/2}$ (fm)
^{12}C	0.1644	0.4988	0.3741	2.407
^{24}Mg	0.1499	0.4012	0.2383	3.050
^4He	0.4229	0	0.7024	1.460

techniques [14] for expression (4), we can obtain the α -cluster distribution function $\rho_c(r')$ as

$$\rho_c(r') = \rho_{0c}(1 + \mu r'^2) \exp(-\xi r' a^2), \quad (5)$$

with $\eta = \lambda - \beta$, $\xi = \beta\lambda/\eta$, and $\mu = 2w\lambda^2/[\eta(2\eta - 3w)]$. Inserting this α -cluster distribution together with the effective α - α interaction potential of Buck *et al.* [15], we can obtain the α - α DFC from Eq. (1).

$$v_{\alpha\alpha}(r) = -122.6225 \exp(-0.22r^2). \quad (6)$$

For the phenomenological potentials, we use slightly modified versions of the potentials previously conducted for this reaction. For the deep potential, we use the potentials of Boztosun and Rae [6], and for the shallow potential, we use the potentials of Sciani *et al.* [2].

The parameters of the potentials are given in Table II. The codes DF POT [16] and FRES CO [17] are used for all calculations.

The experimental data of the $^{12}\text{C} + ^{24}\text{Mg}$ reaction has been analyzed in the laboratory system from 16.0 to 24.0 MeV by using both phenomenological and microscopic potentials within the optical model described here.

To obtain the best fit between the experimental data and the theoretical calculations, we have conducted a χ^2 search to define the parameters of the potentials. For the microscopic DF potentials, we have two free parameters: N_R and W_0 . The normalization factor (N_R) of the real part and the depth (W_0) of the imaginary part have been varied on a grid and the results of this systematic search have shown that the N_R or W_0 parameters cannot be varied continuously and still produce equally satisfying fits. For the normalization factor of the α - α DFC potential, the lowest χ^2 values are generally obtained between 0.7 and 0.9, but we have chosen the parameter $N_{R_{\alpha\alpha}} = 0.72$, which provides a consistent description for all energies. For the NN-DF potential, $N_{R_{NN}} = 0.84$.

Some of the results of our analysis obtained by using microscopic and phenomenological potentials are shown in

Fig. 1 for the individual angular distributions and in Fig. 2 for the fusion cross-section data. Numerical values at energies where the experimental data are available are also shown in Table III for the fusion cross section.

We may infer from the figures that the theoretical results obtained by using the microscopic and phenomenological potentials present more or less the same behavior: It is difficult to see the difference at forward angles since they overlap. The difference becomes apparent at large angles. However, the lowest χ^2 values for the individual angular distributions are provided by the shallow real potential. If we perceive the lowest χ^2 values as the best fit, then we may say that the shallow potential provides the best fit. If we look at the figures, we also perceive that the theoretical results obtained by using the shallow potential give very good agreement with the experimental data at forward, intermediate, and large angles. The magnitude of the cross section is correctly provided and the minima and maxima are at the correct places with the correct phases.

However, the same shallow potential that explains the angular distribution is unable to predict the fusion cross section. The theoretical calculation for the fusion cross section gives a values that rise almost twice that of the experimental value.

Nevertheless, the deep potentials, both microscopic and phenomenological ones, provide a good agreement for the individual angular distributions with acceptable χ^2 values and predict the fusion cross section reasonably well. The magnitude of the cross section is correctly predicted and the minima and maxima are at the correct places with the correct phases. The only discrepancy is at large angles where minima are predicted deeper than the measured data.

These optical model calculations provide the total reaction cross section, but not the fusion cross sections therefore, there is a discrepancy between theoretical predictions and the experimental fusion cross-section data. To obtain the fusion cross section and improve the agreement, we have to either use a model-independent approach such as the one used in Refs. [20,21] or remove the nonelastic cross section from the reaction cross section calculations; we have used the CC model for this purpose and, in our calculations, the fusion cross section is obtained in the following way:

$$\sigma_F = \sigma_R - \sigma_{in}, \quad (7)$$

where σ_F denotes the fusion cross section, σ_R is the total reaction cross section, and σ_{in} is the nonelastic cross section. In the present CC calculations, we describe the interaction

TABLE II. The parameters of the real and imaginary potentials. All imaginary potentials have WS volume shape.

Potential type	V_0 (MeV)	r_V (fm)	a_V (fm)	W_0 (MeV)	r_W (fm)	a_W (fm)
NN	—	—	—	$1.8E + 1.6$	0.30	0.286
α - α	—	—	—	$3.7E - 43.4$	0.30	0.286
WS_D^2	427.0	0.88	1.187	$0.4E + 30.0$	0.30	0.286
WS_S	$49.1 - 0.56E$	1.29	0.400	$0.054E - 0.47$	1.77	0.600

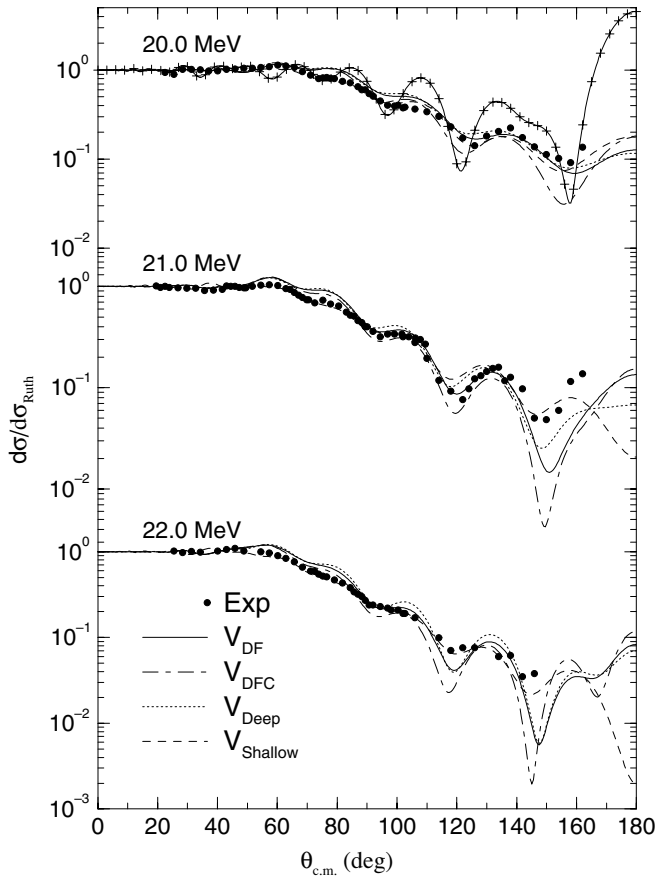


FIG. 1. Optical model elastic scattering results obtained by using NN-DF (solid lines), α - α DFC (dot dashed lines), and phenomenological deep (dotted lines) and shallow (dashed lines) potentials. The solid lines with pluses show the CC prediction of the shallow potential using the short-range imaginary potential at $E_{\text{Lab}} = 20$ MeV (see text). Experimental data are from Ref. [2].

between ^{12}C and ^{24}Mg nuclei with a deformed optical potential. The real potential is assumed to be the square of the Woods-Saxon potential and the imaginary potential has the standard Woods-Saxon volume shape [6].

We assume that the target nucleus ^{24}Mg has a static quadrupole deformation and that its rotation can be described within the framework of the rotational model by deforming

TABLE III. Theoretical reaction and experimental fusion cross sections. Experimental data are taken from Refs. [18,19].

E (MeV)	Exp.	σ (mb)			
		NN-DF	α - α DFC	WS_D^2	WS_S
20.0	198.82	243.23	273.66	236.11	432.50
21.0	243.56	320.64	354.45	311.83	530.18
22.0	331.73	393.56	430.47	371.41	678.13
23.0	426.43	456.69	493.40	443.54	723.56
24.0	435.01	518.43	553.70	493.81	791.99

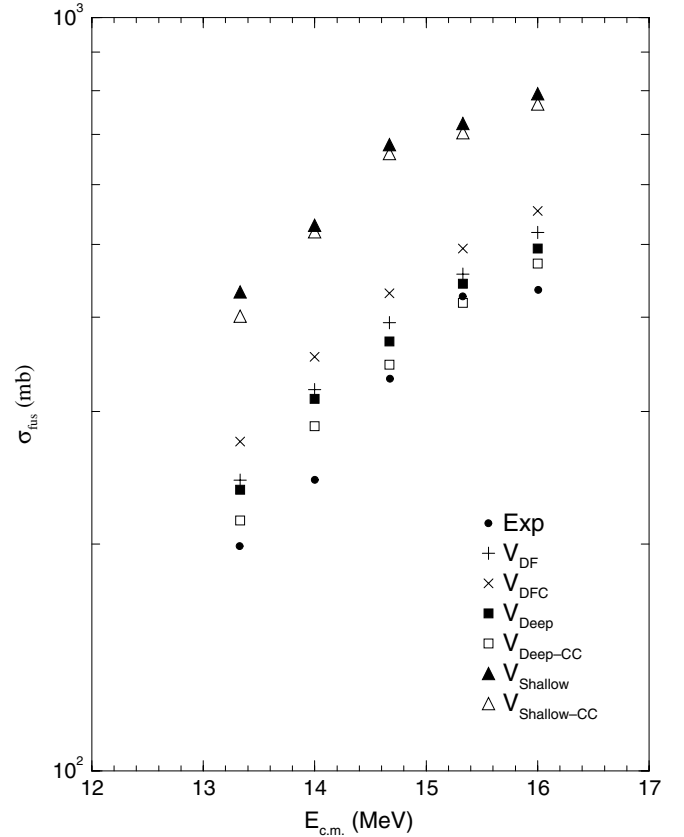


FIG. 2. Experimental fusion cross sections (filled circles) [18, 19] compared with theoretically calculated results using the NN-DF (pluses), the α - α DFC (crosses), and phenomenological deep (filled squares) and shallow (filled upward-pointing triangles) potentials. The CC calculation results using the phenomenological deep (unfilled squares) and shallow (unfilled upward-pointing triangles) potentials are also shown.

the real potential in the following way:

$$R(\theta, \phi) = r_0 A_p^{1/3} + r_0 A_t^{1/3} [1 + \beta_2 Y_{20}(\theta, \phi)], \quad (8)$$

where p and t refer to projectile and target nuclei, respectively, and β_2 is the deformation parameter of ^{24}Mg . We shall use the exact value of β_2 , derived from the deformation length $\delta = 1.50$ fm ($\beta = 0.52$). For the Coulomb deformation, we assume $\beta_2^C + \beta_2^N$.

The results of the CC calculations are shown in Fig. 2 and in Table IV for the fusion calculations. We do not show the elastic scattering angular distribution results obtained since we are mainly interested in the effect of the CC calculation on the fusion data prediction. Nevertheless, the CC results for the elastic scattering angular distribution are reasonable fits to the data. From Fig. 2, it is clear that the inclusion of the 2^+ and 4^+ excited states of ^{24}Mg affects the calculations and gives a better agreement for the fusion calculations in comparison with the optical model. The numerical values of this effect can be seen from Table IV. In this table, we present the optical and CC results for the deep Woods-Saxon squared phenomenological and shallow Woods-Saxon volume potentials. The inclusion of the 2^+ and 4^+ excited states of ^{24}Mg removes flux from

TABLE IV. Comparison of the CC and optical model (OM) fusion cross-section predictions using deep (D) and shallow (S) potentials. Experimental data are from Refs. [18,19]. All cross-section data are in millibarns.

E (MeV)	Exp. σ	OM _S σ_F	CC _D		CC _S		
			σ_F	σ_{2^+}	σ_F	σ_{2^+}	
20.0	198.82	236.11	215.08	22.85	432.50	401.49	26.80
21.0	243.56	311.83	286.72	27.10	530.18	519.42	31.64
22.0	331.73	371.41	346.04	29.86	678.13	659.74	31.71
23.0	426.43	443.54	418.00	32.33	723.56	703.22	39.64
24.0	435.01	493.81	471.67	34.10	791.99	767.74	45.05

the elastic channel and the CC results for the fusion data are in better agreement than those of the optical model. From Table IV, it may be observed that, although the optical model prediction is around $\sigma_F = 236.11$ mb at $E_{\text{Lab}} = 20.0$ MeV, it becomes $\sigma_F = 215.08$ mb after the inclusion of the 2^+ and 4^+ excited states of ^{24}Mg . The effect is around 22.85 mb, which makes the theoretical CC prediction in better agreement with the experimental data. The same effect has been also observed for the shallow real potential, the CC calculations improve the agreement with the experimental fusion data, but it is still far from being comparable with the prediction of the deep potentials.

We have noticed that the failure of the shallow potential may be related to the long-range imaginary potential we have used in the calculations. Because of this long-range imaginary potential, we cannot obtain satisfactory agreement with the fusion cross section. However, when we reduce the range of the imaginary potential and use one similar to the deep potential model, we get better agreement with the fusion data, but this time we are unable to obtain good agreement with the elastic scattering angular distribution. This is illustrated in Fig. 1 at $E_{\text{Lab}} = 20.0$ MeV. In this figure, the solid line with the pluses shows the prediction of a short-range imaginary potential as used in the deep Woods-Saxon squared potential. The parameters are given in Table II. As a result, we have reached the conclusion that it is not possible to explain the

elastic scattering angular distribution and fusion cross section simultaneously by using a shallow real potential.

Describing the $^{12}\text{C} + ^{24}\text{Mg}$ system theoretically has been very difficult since the experimental data show very oscillatory features near the Coulomb barrier at very low energies and a striking backward rise and oscillatory features at forward, intermediate, and backward angles at high energies. In this Brief Report, we have shown a consistent description of the elastic scattering of the $^{12}\text{C} + ^{24}\text{Mg}$ system at energies around and above the Coulomb barrier, from 16.0 to 24.0 MeV, in the laboratory system by using the NN-DF and α - α DFC potentials in the optical model calculations. This constitutes the first detailed application of the folding model. All potentials, both deep and shallow, have provided excellent agreement with the experimental data for the elastic scattering individual angular distributions at different laboratory energies; however, only deep potentials explain the angular distributions and fusion cross-section data simultaneously. As we have argued here, the origin of the large difference between deep and shallow potentials for the fusion cross-section data is related to the long-range imaginary potential. This work clearly demonstrates the inadequacy of using shallow potentials in describing such nuclear reactions and underlines the validity of the double folding potentials.

This project is supported by TÜBİTAK, Grant No. TBAG-2398, and by Erciyes University, FBT-04-15.

- [1] M. E. Brandan and G. R. Satchler, Phys. Rep. **285**, 143 (1997).
[2] W. Sciani, A. Lepine-Szily, F. R. Lichtenhaeler, P. Fachini, L. C. Gomes, G. F. Lima, M. M. Obuti, J. M. Oliveira Jr., and A. C. C. Villari, Nucl. Phys. **A620**, 91 (1997).
[3] A. Lepine-Szily, W. Sciani, Y. K. Watari, W. Mittig, F. R. Lichtenhaeler, M. M. Obuti, J. M. Oliveira Jr., and A. C. C. Villari, Phys. Lett. **B304**, 45 (1993).
[4] R. Lichtenhaler Filho, A. Lepine-Szily, A. C. C. Villari, and O. P. Filho, Phys. Rev. C **39**, 884 (1989).
[5] J. Carter, R. G. Clarkson, V. Hnizdo, R. J. Keddy, D. W. Mingay, F. Osterfeld, and J. P. F. Sellschop, Nucl. Phys. **A273**, 523 (1976).
[6] I. Boztosun and W.D.M. Rae, Phys. Rev. C **64**, 054607 (2001).
[7] S. Erturk, I. Boztosun, Y. Kucuk, M. Karakoc, and S. Aydin, J. Phys. G **31**, S1837 (2005).
[8] M. Karakoc, M.Sc. thesis, Erciyes University, 2005.
[9] W. D. M. Rae, Int. J. Mod. Phys. A **3**, 1343 (1988).
[10] M. Freer and A. C. Merchant, J. Phys. G **23**, 261 (1997).
[11] M. El-Azab Farid, Z. M. M. Mahmoud, and G. S. Hassan, Nucl. Phys. **A691**, 671 (2001).
[12] M. El-Azab Farid and M. A. Hassanain, Nucl. Phys. **A678**, 39 (2000).
[13] RIPL-2, Nuclear Matter Densities, IAEA, <http://www-nds.iaea.org/RIPL-2/>.
[14] G. R. Satchler and W. G. Love, Phys. Rep. **55**, 183 (1979).
[15] B. Buck, H. Friedrich, and C. W. W. Wheathly Nucl. Phys. **A275**, 246 (1977).
[16] J. Cook, Comput. Phys. Commun., **25**, 125 (1982).
[17] I. J. Thompson, computer code FRESKO, unpublished.
[18] A. Iwamoto, P. Moeller, J. R. Nix, and H. Sagawa, Nucl. Phys. **A596**, 329 (1996).
[19] S. Gary and C. Volant, Phys. Rev. C **25**, 1877 (1982).
[20] J. T. Holdeman and R. M. Thaler, Phys. Rev. Lett. **14**, 81 (1965); Phys. Rev. **139**, B1186 (1965).
[21] T. Yamaya *et al.*, Phys. Lett. **B417**, 7 (1998).